Heterogeneity of hypochlorous acid production in individual neutrophil phagosomes revealed by a rhodamine-based probe

Received for publication, July 9, 2018, and in revised form, August 12, 2018 Published, Papers in Press, August 22, 2018, DOI 10.1074/jbc.RA118.004789

Amelia M. Albrett[1], **Louisa V. Ashby**[2], **Nina Dickerhof**, **Anthony J. Kettle**, and **Christine C. Winterbourn**[3]

From the Department of Pathology and Biomedical Science, Centre for Free Radical Research, University of Otago Christchurch, Christchurch 8140, New Zealand

Edited by Ruma Banerjee

The rhodamine-based probe R19-S has been shown to react with hypochlorous acid (HOCl) to yield fluorescent R19, but not with some other oxidants including hydrogen peroxide. Here, we further examined the specificity of R19-S and used it for real-time monitoring of HOCl production in neutrophil phagosomes. We show that it also reacts rapidly with hypobromous acid, bromamines, and hypoiodous acid, indicating that R19-S responds to these reactive halogen species as well as HOCl. Hypothiocyanous acid and taurine chloramine were unreactive, however, and ammonia chloramine and dichloramine reacted only very slowly. MS analyses revealed additional products from the reaction of HOCl with R19-S, including a chlorinated species as a minor product. Of note, phagocytosis of opsonized zymosan or *Staphylococcus aureus* by neutrophils was accompanied by an increase in R19 fluorescence. This increase depended on NADPH oxidase and myeloperoxidase activities, and detection of chlorinated R19-S confirmed its specificity for HOCl. Using live-cell imaging to track individual phagosomes in single neutrophils, we observed considerable heterogeneity among the phagosomes in the time from ingestion of a zymosan particle to when fluorescence was first detected, ranging from 1 to >30 min. However, once initiated, the subsequent fluorescence increase was uniform, reaching a similar maximum in ~10 min. Our results confirm the utility of R19-S for detecting HOCl in real-time and provide definitive evidence that isolated neutrophils produce HOCl in phagosomes. The intriguing variability in the onset of HOCl production among phagosomes identified here could influence the way they kill ingested bacteria.

Since Klebanoff (1–5) first demonstrated the microbicidal activity of myeloperoxidase (MPO),[4] hydrogen peroxide (H_2O_2), and chloride, there is a general consensus that the product of this reaction, hypochlorous acid (HOCl), plays an important role in the killing of bacteria by neutrophils. However, demonstrating that HOCl is produced when neutrophils ingest bacteria and dissecting its role in killing has been challenging, due to difficulties in detecting this highly reactive species. Several studies involving analysis of phagosomal contents provide evidence that HOCl is produced (3, 6–10) but there is debate about how much, whether this is sufficient to kill, and whether it does so directly. Others query whether HOCl is produced at all (11, 12). To gain a greater understanding of how MPO functions during phagocytosis, real-time monitoring of HOCl at intracellular sites is needed.

In recent years, a plethora of probes for HOCl has been developed (13–18). One of these, R19-S, is a rhodamine-based dye developed by Chen and colleagues (13, 19). The dye is initially a nonfluorescent thiospirolactone that gets switched on to a highly fluorescent rhodamine structure (R19) upon oxidation by HOCl (Fig. 1). Chen *et al.* (13) showed a positive response in phagocytosing neutrophils, and established specificity relative to H_2O_2, superoxide, hydroxyl and peroxyl radicals, singlet oxygen, and reactive nitrogen species. They also showed that, in contrast to some of the other probes, R19-S is not a direct substrate for MPO. However, none of these probes has been tested for specificity against hypobromous acid (HOBr), hypoiodous acid (HOI), and hypothiocyanous (HOSCN), which are generated by MPO and other mammalian peroxidases, or against the chloramines or bromamines that are produced in secondary reactions with amines or ammonia (Reactions I and II for HOCl).

$$HOCl + RNH_2 \rightarrow RNHCl + H_2O$$

Reaction I

$$HOCl + RNHCl \rightarrow RNCl_2 + H_2O$$

Reaction II

We have extended the initial studies with R19-S to characterize the products of the reaction using MS and to establish that the probe can react with some of these other peroxidase products. We have also used it for in-depth studies of MPO-dependent HOCl production by phagocytosing neutrophils. We

This work was supported by the Health Research Council of New Zealand. The authors declare that they have no conflicts of interest with the contents of this article.

This article contains Movie S1.

[1] Present address: Landcare Research, P. O. Box 69040, Lincoln 7640, New Zealand.

[2] Previously published as Louisa V. Forbes.

[3] To whom correspondence should be addressed: Dept. of Pathology and Biomedical Science, University of Otago Christchurch, P. O. Box 4345, Christchurch 8140, New Zealand. Tel.: 64-3-364-0564; E-mail: christine.winterbourn@otago.ac.nz.

[4] The abbreviations used are: MPO, myeloperoxidase; DPI, diphenyleneiodonium chloride; HBSS, Hanks' buffered saline solution; SOD, superoxide dismutase; TX1, 3-isobutyl-2-thioxo-7*H*-purine-6-one; HX1, 2-(3,5-bistrifluoromethylbenzylamino)-6-oxo-1*H*-pyrimidine-5-carbohydroxamic acid; DIC, differential interference contrast; NOX, NADPH oxidase.

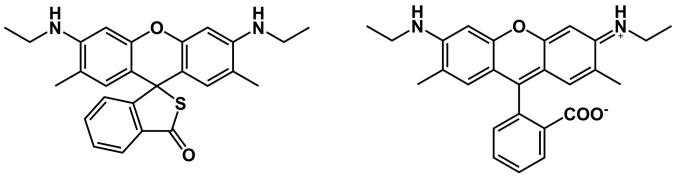

Figure 1. Structures of R19-S (*left*) and R19 (*right*).

show that R19-S oxidation can be followed by flow cytometry or fluorescence microscopy to track intracellular and extracellular HOCl, and with live-cell imaging to follow production in real-time in individual phagosomes. This has revealed heterogeneity between individual phagosomes in the time course of HOCl production following ingestion of zymosan particles, with some showing a rapid increase in fluorescence and others remaining nonfluorescent over the 30-min recording period.

Results and discussion

Products and reactivity of R19-S with HOCl

Chen *et al.* (13) have shown that R19-S reacts with HOCl to give the fluorescent product, R19 (Fig. 1). To gain an appreciation of whether multiple products are formed, we analyzed the reaction using LC-MS. R19-S (mass 430 Da, Fig. 2*A*) gave a peak at 15 min with m/z of 431 representing the singly charged ion. Addition of HOCl at a molar ratio of 0.5:1 resulted in loss of a quarter of the R19-S peak, consistent with a 2:1 HOCl:R19-S stoichiometry. One major product peak was observed at 12.8 min, which contained three main ion species with m/z of 415, 430, and 447 (Fig. 2*B*). The highest intensity m/z 415 peak can be assigned to the singly charged $[M+H]^+$ of R19 (mass 414 Da). The other ions are consistent with the doubly charged $[M+2H]^{2+}$ of a covalent R19-S dimer (mass $2 \times 430 - 2H$) and singly charged $[M+H]^+$ of R19+O (mass 430 + 16). Although the structures of the product species were not characterized further, the dimer could be a disulfide and the M+16 peak a sulfoxide, likely intermediates or products in the multistep oxidation of R-19S. At high ratios of HOCl:R19-S, R19 underwent further oxidation to nonfluorescent species.

Upon HOCl treatment, a small shoulder appeared at 15.8 min. This contained ions with the m/z of 465 and 467 at a ratio of 3:1, consistent with the singly charged $[M+H]^+$ of the two isotopes of a chlorinated R19-S species, designated as R19S-Cl (Fig. 2*B*). Although a minor product, the definitive chlorine 3:1 footprint is a marker of oxidation by HOCl.

To determine how effectively R19-S can compete for HOCl in the presence of physiological targets, we carried out the reaction in the presence of varying concentrations of a range of compounds that react with HOCl with known rate constants. For the reaction of 5 μM HOCl with 10 μM R19-S, the addition of *N*-α-acetyl-Lys ($k = 7.9 \times 10^3\ M^{-1}\ s^{-1}$), taurine ($k = 4.8 \times 10^5\ M^{-1}\ s^{-1}$), or *N*-acetyl-Trp ($k = 1.1 \times 10^4\ M^{-1}\ s^{-1}$) (20) at 20 μM, caused almost complete inhibition. However, as shown in Fig. 3, the data did not fit a simple competitive model, with *N*-α-acetyl-Lys showing the same inhibition curve with 10 μM as with 100 μM R19-S. This could be explained by the reaction of R19-S involving multiple steps, with a faster first step generating an intermediate, which is scavenged by the other compounds. Further kinetic analyses are required to elucidate the mechanism and obtain rate constants. However, the observation that low concentrations of amino acids were able to inhibit fluorescence indicates that one step may be relatively slow, and at concentrations typically used in cell studies R19-S would have to compete with multiple physiological targets.

Reactivity of R19-S with other hypohalous acids and haloamines

We compared the reactivity R19-S with HOCl, HOBr, HOSCN, HOI, chloramines, and bromamines. With equimolar HOCl and R19-S, the reaction was rapid and complete within 5 min (Fig. 4). HOBr also reacted rapidly but gave only half the fluorescence yield of HOCl. HOSCN gave almost no reaction even after 1 h, although a gradual response was seen at higher concentrations. HOI reacted rapidly to give very high fluorescence, with absorbance changes indicating that (possibly iodinated) products other than R19 were formed. To test for chloramine and bromamine reactivity, we selected taurine derivatives, as they are among the less reactive amino acid haloamines, and the highly reactive mono- and di-chloramines of ammonia (21, 22). Taurine chloramine did not react with R19-S, and although the ammonia chloramines did react, their reactions were very slow and at 1 h gave only 12 and 16%, respectively, of the fluorescence seen with HOCl within 5 min. However, taurine bromamine reacted rapidly and gave twice the yield seen with HOCl. The reason for the different yields with the brominated oxidants was not explored but it is likely that they reflect formation of different proportions of R19 and the other nonfluorescent products.

It is apparent from our results that R19-S is not specific for HOCl, and in systems where other peroxidase products are generated, they should be considered as potential probe oxidants. However, with neutrophils it is reasonable to assume that the probe detects HOCl production. HOBr and HOI are minor MPO products at physiological bromide and iodide concentrations. Although chloramines are likely to be formed from HOCl in neutrophils (23), their low or negligible reactivity means they should contribute little to probe oxidation. On the other hand, eosinophil peroxidase and peroxidasin use bromide as a favored substrate, and R19-S will detect HOBr and bromamines in systems where these peroxidases are active.

We confirmed previous findings (13) that R19-S does not react with H_2O_2 or with MPO in the absence of chloride, and observed that the fluorescence yield was similar when HOCl was added as a reagent or was generated by MPO, chloride, and an equivalent concentration of H_2O_2 (not shown). It has recently been reported that a pH of 8.5–9 is achieved within neutrophil phagosomes (12). We therefore tested the reactivity of HOCl with R19-S at a higher pH. Under conditions similar to those in Fig. 4 the fluorescence yield at pH 8.5 was 110 ± 10% of that at pH 7.4. At pH 8.5, H_2O_2 (100 μM) still gave no reaction.

Detection of HOCl production by stimulated neutrophils using R19-S

Detection of extracellular and intracellular HOCl by fluorimetry—The original study with R19-S used live cell imaging to detect HOCl in neutrophils (13). We tested whether it could be used with fluorimetry or flow cytometry. For fluorimetry, neu-

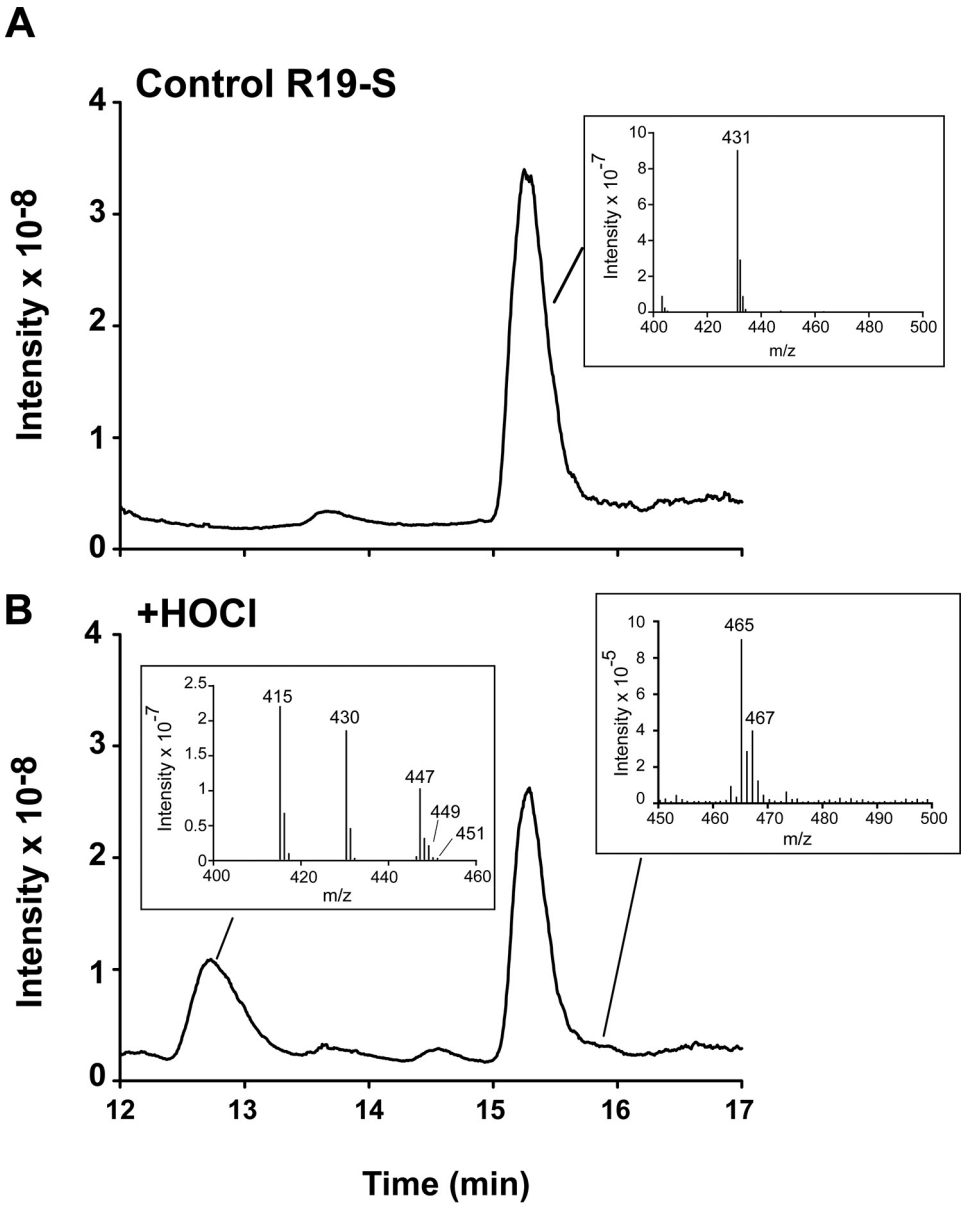

Figure 2. Detection of multiple products formed from R19-S and HOCl by LC-MS. *A* and *B*, total ion chromatograms of (*A*) R19-S (20 μM) before and (*B*) after incubation with HOCl (10 μM). *Insets* show mass spectra for R19-S (431), and the peaks containing R19 (415) and R19S-Cl (465/467).

trophils were stimulated to ingest opsonized zymosan in the presence of R19-S in 96-well plates. Little fluorescence was seen in resting cells, but with zymosan added there was an initial lag, then a progressive increase in R19 fluorescence over time (Fig. 5*A*). The NADPH oxidase inhibitor, diphenyleneiodonium chloride (DPI), completely suppressed the response. This method measures both intracellular HOCl and HOCl produced by the neutrophils and released into the medium. To measure predominantly intracellular HOCl, we added methionine, an efficient HOCl scavenger that should act outside the cells and have little intracellular impact. Most of the signal was suppressed. Furthermore, when the cells and supernatant were separated at the end of the experiment, the majority of the fluorescence was extracellular and prevented by methionine (Fig. 5*B*). The lower fluorescence of the cell fraction was relatively resistant to methionine. Thus neutrophil HOCl production can be measured by this method, but it is difficult to detect intracellular events.

NOX2 and MPO dependence of HOCl production demonstrated with flow cytometry—For flow cytometry, opsonized zymosan (20:1) was added to the neutrophils, with methionine included to scavenge extracellular HOCl. There was a pronounced increase in R19-S fluorescence in the stimulated but not resting cells that was totally inhibited by DPI (Fig. 6, *A* and *B*). Imaging of the neutrophils after 30 min showed phagocytosis of multiple zymosan particles and R19-S fluorescence associated with most but not all phagosomes (Fig. 6*B*). By flow cytometry, two populations of cells with different fluorescent intensity were apparent, perhaps representing varying degrees of phagocytosis or NOX activity. Cellular R19-S fluorescence increased rapidly after zymosan addition and slowed down by 30 min (Fig. 6*C*). A shorter lag was seen than in Fig. 5, probably

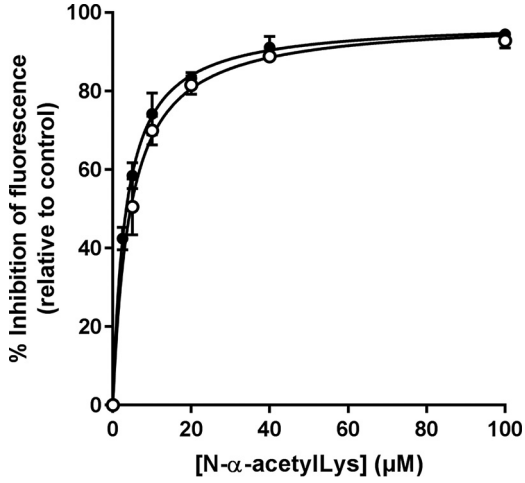

Figure 3. Assessment of reaction kinetics between R19-S and HOCl by competition with *N*-α-acetyl-lysine. 10 (○) or 100 μM (●) R19-S was mixed with increasing concentrations of *N*-α-acetyl-Lys in PBS, then 5 μM HOCl was added while vortexing. Fluorescence (excitation 515/emission 550) was measured immediately upon transfer of the reaction mixture into a platereader. The fluorescence in the absence of *N*-α-acetyl-Lys is the control value for formation of fluorescent R19. Each data point is the mean ± S.D. of the % inhibition measured in three separate experiments.

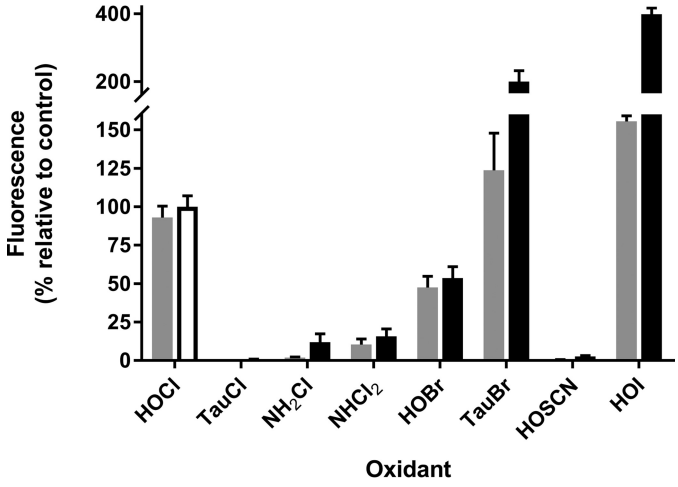

Figure 4. Fluorescence response of R19-S to hypohalous acids, chloramines, and bromamines. Reactions were carried out in PBS by mixing 10 μM R19-S and 10 μM of each oxidant while vortexing. The fluorescence response was measured at 5 (*gray bars*) and 60 min (*black bars*) using a platereader. *TauCl*, taurine chloramine; *TauBr*, taurine bromamine. Results are expressed as a percent of the fluorescence observed with HOCl at 60 min (*white-filled bar*) and are mean ± S.D. from three independent experiments. The products with HOI, as well as having high fluorescence, showed a different UV-visible spectrum from that with HOCl, with higher absorbing peaks in the 515 nm excitation band region.

because phagocytosis was more efficient in the rotating tubes used for these experiments than in the more static plate format.

Consistent with the signal being due to HOCl, fluorescence was much lower when the neutrophils were suspended in chloride-free buffer (Fig. 6*C*). Definitive proof that HOCl was responsible for oxidation was obtained by LC-MS analysis of the R19-S oxidation products. Both R19 and the chlorinated product R19S-Cl were detected and decreased in parallel in the presence of DPI (Fig. 6*D*).

An increase in intracellular R19 fluorescence was also detectable in neutrophils following phagocytosis of *Staphylococcus aureus* (Fig. 6*E*). The response followed a similar time course to

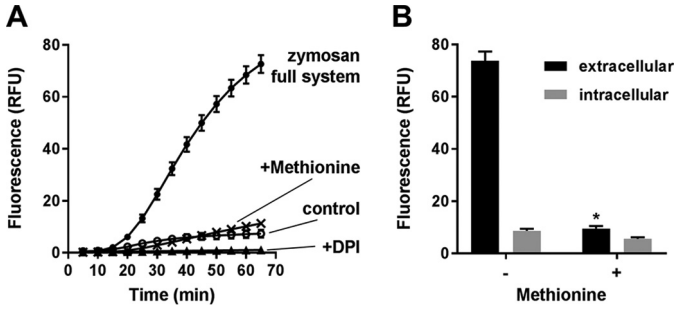

Figure 5. Detection of R19-S oxidation by phagocytic neutrophils using fluorimetry. *A*, total R19-S fluorescence detected for neutrophils stimulated with opsonized zymosan (1:20) in the absence (●) or presence of DPI (▲) or methionine (×). Control cells (○) have no zymosan added. Incubations were carried out in HBSS in 96-well plates and fluorescence (excitation 515/emission 550 nm) was measured at intervals up to 65 min. *B*, fluorescence of extracellular (*black*) and intracellular (*gray*) fractions prepared from neutrophils after 70 min incubation with zymosan ± methionine (1 mM) as in *A*. Statistically significant decrease in fluorescence of the extracellular (*, $p = 0.013$, paired *t* test) but not intracellular fractions. Results are mean ± S.E. from three independent experiments.

that with zymosan. The signal with bacteria was lower, consistent with their smaller size giving smaller phagosomes. When neutrophils from a severely MPO-deficient individual (2–3% of normal activity) (24) were stimulated with *S. aureus*, the fluorescence response was less than 15% of that with normal neutrophils, thus establishing MPO-dependence.

We also determined the effect on intracellular HOCl production of two potent inhibitors of MPO: 2-thioxanthine TX1, which acts as a suicide inhibitor, and hydroxamate HX1, which is a tight binder (25, 26). Flow cytometry analyses following ingestion of *S. aureus* (Fig. 6*F*) showed that both TX1 and HX1 decreased fluorescence by ~50%. Previously, these inhibitors have been shown to fully inhibit HOCl production by MPO (27). Consistent with this, we measured complete inhibition of extracellular R19 fluorescence with phorbol 12-myristate 13-acetate-stimulated cells (not shown). Compared with the near complete lack of R19-S oxidation in MPO-deficient cells, these potent inhibitors were unable to completely suppress the activity of MPO released into the neutrophil phagosome. A possible explanation is low permeability, but other contributors may be the high MPO concentration in the phagosome (6).

Superoxide reacts directly with HOCl and interacts with MPO to modulate HOCl production (28, 29). To test whether these interactions affect HOCl production in the phagosome, where large amounts of superoxide are generated, we attached SOD to the surface of the zymosan so that it would be taken up during phagocytosis and examined the effect on R19-S fluorescence. Analyses performed with dihydroethidium as a superoxide detector (30) showed that the attached SOD significantly decreased the fluorescent signal of the cells (Fig. 7). Coupled SOD gave a small but significant increase in R19 fluorescence above either normal zymosan, or zymosan coupled to inactivated SOD. These results are consistent with the superoxide generated in the phagosome causing a slight decrease but not a major impact on the availability of HOCl in the phagosome.

Following phagosomal HOCl production by live-cell imaging—The images in Fig. 6*B* show clearly that R19-S fluorescence is closely associated with individual phagosomes following inges-

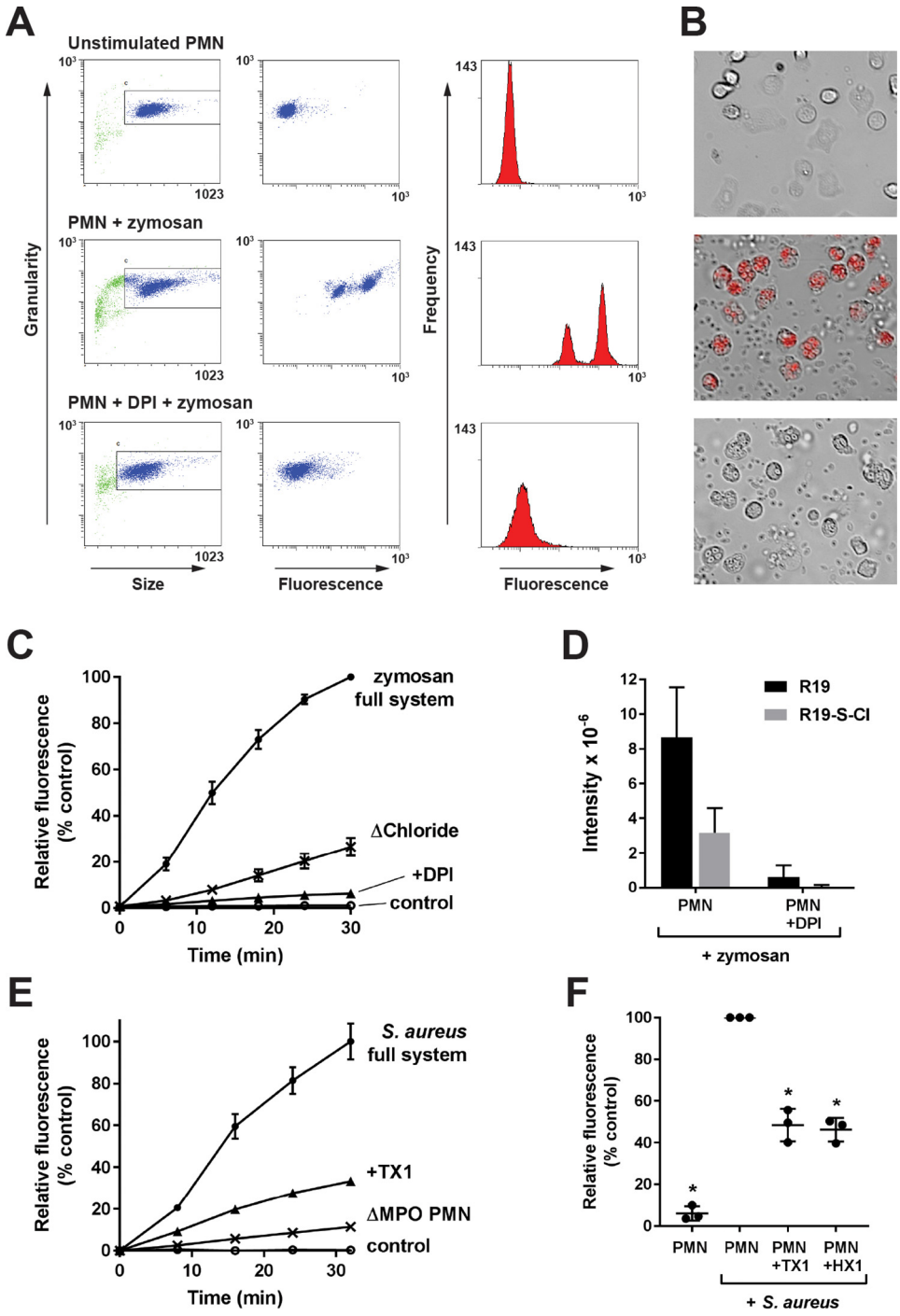

Figure 6. Detection of HOCl production within neutrophils stimulated by zymosan or bacteria, and dependence on NOX2 activity and MPO. *A,* flow cytometry scattergrams from unstimulated neutrophils (polymorphonuclear (*PMN*), *top*) and neutrophils stimulated with 20:1 zymosan in HBSS containing 1 mM methionine, in the absence (*middle*) and presence (*bottom*) of DPI, recorded after 30 min. The gated neutrophil populations (*left panels*) were analyzed for R19 fluorescence (*middle panels*) and represented as histograms (*right panels*). *B,* corresponding merged R19 fluorescence (*red*) and bright field (Cy3/DIC) images of neutrophils treated for 30 min as in *A* and recorded by fluorescence microscopy. *C,* time course of mean fluorescence increase for the entire neutrophil population treated as in *A* for neutrophils that were unstimulated (○) or stimulated with zymosan in the absence (●) or presence (▲) of DPI or treated in chloride-free gluconate buffer (×). Results show mean ± S.E. from three independent experiments. Data points are normalized against the fluorescence (93 FU) of phagocytic neutrophils at 30 min. *D,* detection of R19 and R19S-Cl by LC-MS in neutrophils (10^6) harvested and lysed following 30 min stimulation as in *A*. Data are means of duplicates ± S.D. from a representative of two independent experiments. *E,* R19-S fluorescence increase over time measured by flow cytometry as in *A* following addition of *S. aureus* (at 10:1) to normal neutrophils in the absence (●) or presence (▲) of MPO inhibitor TX1, and neutrophils from an individual with MPO deficiency (×), compared with normal neutrophils incubated without bacteria (○). Results show mean ± S.D., the mean maximum fluorescence of normal neutrophils after phagocytosing bacteria was 13 FU. *F,* inhibition of R19 fluorescence by MPO inhibitors. Neutrophils were incubated with *S. aureus* (at 10:1) in the presence of 1 mM methionine for 30 min with and without pre-exposure for 10 min to 10 μM TX1 or HX1. *, significance relative to *S. aureus* with no inhibitor as determined by one-way analysis of variance with Dunnett's post-test correction for multiple comparisons ($p \leq 0.0001$).

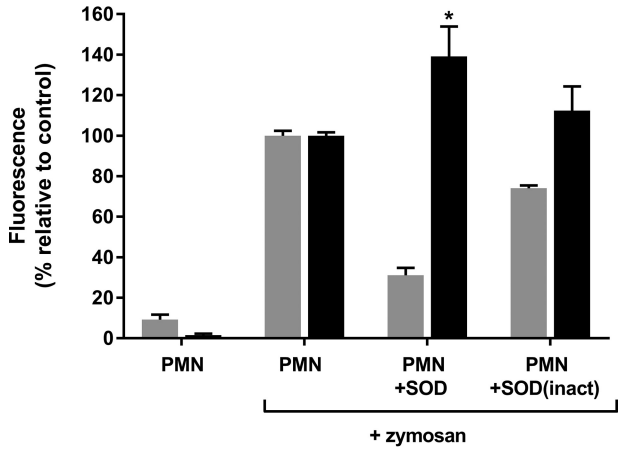

Figure 7. Effect of delivering zymosan-bound SOD to neutrophil phagosomes. Neutrophils (5×10^6/ml) were pretreated with either 10 μM dihydroethidium (*gray bars*) or 10 μM R19-S (*black bars*), and then incubated with the zymosan preparations (5×10^7/ml) for 30 min at 37 °C. Mean intracellular fluorescence of the neutrophils was measured by flow cytometry, and values are expressed relative to the fluorescence with normal zymosan. *, dihydroethidium fluorescence significantly decreased and R19 fluorescence significantly increased with SOD-linked zymosan compared with phagocytosis of normal zymosan or inactive SOD-zymosan ($p < 0.01$, paired *t* test). Results are mean ± S.D. from three separate experiments.

tion of zymosan particles. To gain a greater insight into HOCl production within the neutrophils, time-lapse videos were taken (see Movie S1) with a sequence of shots taken over a 30-min period as shown in Fig. 8*A*. Over time, more neutrophils and zymosan particles entered the frame as they settled to the base of the dish, with 15 neutrophils visible by 30 min in the field shown. Each neutrophil sequentially took up multiple particles into individual phagosomes, and after a lag period there was a progressive increase in fluorescence intensity. This process appeared to occur independently in each phagosome.

To gain quantitative data on the time course of ingestion and fluorescence, we used imaging software to track individual phagosomes. Two parameters were monitored, the time between phagocytosis and detectable fluorescence, and the time between detectable and maximal fluorescence. As shown in Fig. 8*B*, the lag-time between zymosan ingestion and detectable fluorescence varied widely. Most phagosomes became fluorescent within 10 min of ingestion (average lag-time 5.8 min) but some took longer and remained nonfluorescent at the end of the video recording. The observed variability existed within each neutrophil rather than between neutrophils. As shown in Fig. 8*C*, for the cells in which multiple phagosomes were followed, some showed uniformly short lags, but those containing phagosomes that responded slowly invariably contained others that showed a rapid response.

Development of fluorescence within each phagosome was much more uniform (Fig. 8*D*). As soon as the signal was detectable, it increased rapidly over about 2 min, then continued to increase at a slower rate to reach a maximum that remained steady for the duration of the time-lapse events. The whole process was complete within about 10 min. A possible explanation for the plateauing of fluorescence is that all the R19-S was consumed. However, this is unlikely because when MPO was partially inhibited by TX1, both the rate of increase and the maximum fluorescence in each phagosome were decreased (64 and 52%, respectively) but the kinetic profile was similar (Fig. 8*D*). The percentage of fluorescent phagosomes was not altered on addition of TX1. Furthermore, R19-S was still detectable by LC-MS in the experiment described in Fig. 6*D*, indicating that it should not have been limiting. It is likely, therefore, that the R19 fluorescence signal monitors the duration of HOCl production in each phagosome.

Conclusions

Our results provide good validation of R19-S as a detector of real-time HOCl production in neutrophils. We have also shown that the probe reacts well with HOBr and bromamines. This extends its usefulness for monitoring systems such as eosinophils or collagen IV-producing cells, where these species are produced by eosinophil peroxidase or peroxidasin. The nonspecificity of the probe is unlikely to be an issue with isolated neutrophils. However, in more complex systems such as whole animals it will not distinguish which oxidant is being detected. We have shown that R19 is not the only product, and that competing reactions in a physiological environment should result in R19-S capturing only a fraction of the HOCl being generated. Although this makes absolute quantification difficult, it has an advantage for neutrophil studies, as otherwise the probe could be consumed too rapidly.

Our results with R19-S provide convincing evidence that HOCl is produced within phagocytosing neutrophils, and substantiate other studies where this has been measured less directly (3, 8, 18, 31, 32). HOCl production can be monitored in a fluorescence platereader, but intracellular probe oxidation is best monitored by flow cytometry or live-cell imaging. Ingestion of zymosan can be readily followed as well as the lower fluorescence associated with uptake of smaller bacteria.

The value of live-cell imaging is that individual phagosomes can be tracked independently within the same neutrophil. The most striking feature of these results was the heterogeneity of phagosomes. Quantitative analysis gave a duration of HOCl production from the time of first detection of ~10 min. This, as well as the amount of signal produced, was reasonably consistent between phagosomes, and agrees well with other less direct measurements of the length of the neutrophil oxidative burst (33). However, there was surprising variability in the time between phagocytosis of a zymosan particle and the onset of R19-S oxidation. This ranged from a minute to longer than the 30-min video recording. Our data suggest that if monitored for long enough all the phagosomes would eventually show detectable HOCl, but it is possible that some would never do so. Contributors to the lag could be assembly of the membrane-bound and soluble NOX2 components required for activation and superoxide generation, fusion of azurophil granules and release of their MPO, and initial scavenging of HOCl by highly reactive targets. Although it is likely that R19-S competes for only a fraction of the HOCl produced, it seems unlikely that the availability of scavengers would differ sufficiently between phagosomes to account for the variations in lag. Non-uniform distribution of the cell-permeable dye also seems unlikely. A more likely scenario is that there is variability in the timing of NOX2 assembly, with the possibility that this does not occur in every phagosome. This is supported by the findings of Dinauer and

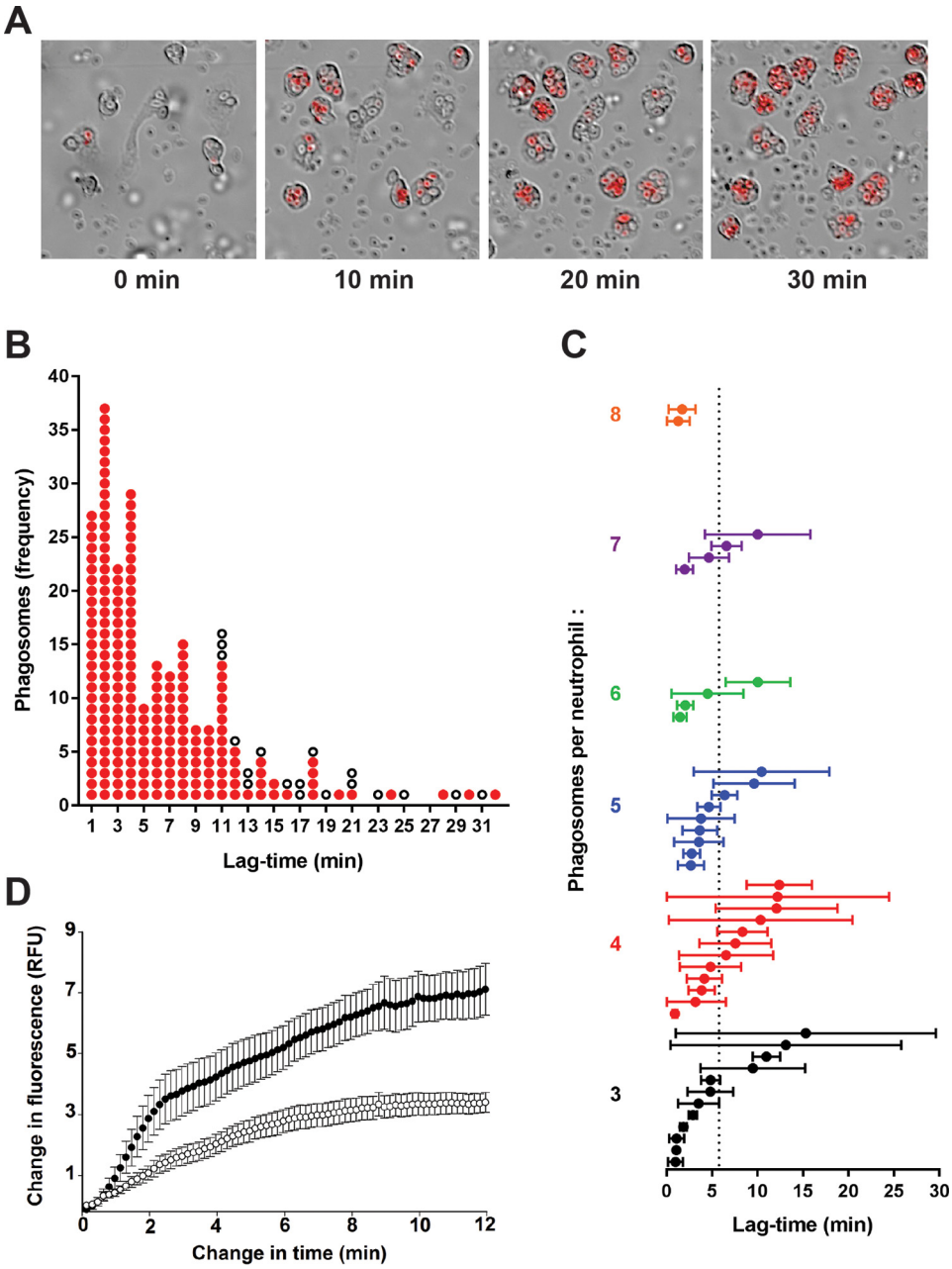

Figure 8. HOCl production in individual phagosomes of neutrophils stimulated with opsonized zymosan as assessed by live-cell fluorescence imaging. *A,* time-lapse frames at 0, 10, 20, and 30 min from a movie of neutrophils and R19-S incubated with zymosan particles (1:20). Images show merged Cy3/DIC channels, and the full video is available in Movie S1. *B,* analysis of 233 phagosomes from 54 neutrophils monitored in a typical experiment as in *A*. The change in time is the interval between frames when phagocytosis of a particle occurred and R19 fluorescence first appeared. Each phagosome is plotted as a *red dot* against the time it took to start fluorescing. *White dots* represent phagosomes that formed in the first 20 min of the movie, but failed to fluoresce within the plotted time change until the end of the video. *C,* mean lag-times for fluorescence in neutrophils with three or more phagosomes. Each plotted *circle* represents one of 43 monitored neutrophils, where the mean lag-time ± S.D. was calculated for the initial appearance of detectable fluorescence in its phagosomes after ingestion of a zymosan particle. The neutrophils are arranged vertically in increasing order of how many phagosomes were monitored per neutrophil. The mean lag-time across all 197 fluorescent phagosomes was 5.8 min, indicated by the *dotted line*. *D,* the development of fluorescence in phagosomes was compared for neutrophils incubated with zymosan in the absence (●) or presence (○) of MPO inhibitor TX1 (10 μM). The increase in fluorescence intensity is plotted against time, starting from when it was first detectable. Data points are the mean ± S.E. from 20 phagosomes analyzed in three separate experiments. A low fluorescence intensity was set and each video frame was analyzed until maximum fluorescence was obtained using Cell R software.

co-workers (34), who followed the assembly of NOX2 in neutrophils after particle ingestion, and showed that within the same cell the cytoplasmic components $p47^{phox}$ and $p67^{phox}$ migrated to the membranes of some but not other individual phagosomes. This intriguing observation has implications for possible heterogeneity in the killing of ingested microorganisms.

Another useful application of R19-S is for monitoring how well small molecule inhibitors act against MPO within the neutrophil. Various compounds that inhibit MPO are currently used to probe the involvement of MPO in experimental systems or are in development as potential drugs for use in conditions such as cardiovascular disease where MPO is implicated in the pathology (25, 26, 35, 36). Our results show that even potent

inhibitors of MPO in isolation are only partially effective inside the cell. This could be desirable for therapeutic applications aimed at inhibiting extracellular MPO without affecting microbicidal activity, but in other applications it could be a disadvantage. A rapid screen with R19-S and flow cytometry would enable intracellular potency to be assessed.

Experimental procedures

Reagents

R19-S was purchased from FutureChem Co. (Seoul, Republic of Korea) or synthesized as described (19). Stock solutions of ~1 mM in acetonitrile were prepared weekly with concentrations determined by measuring absorbance at 308 nm (ϵ_{308} 14,000 M^{-1} cm^{-1}).

Myeloperoxidase inhibitors TX1 (3-isobutyl-2-thioxo-7*H*-purine-6-one) and HX1 (2-(3,5-bistrifluoromethylbenzylamino)-oxo-1H-pyrimidine-5-carbohydroxamic acid) were gifts from AstraZeneca (Mölndal, Sweden). Hydrogen peroxide (H_2O_2 30% solution, Lab-Serv Pronalys) was purchased from Biolab (Auckland, New Zealand). Other chemicals were from Sigma.

Sodium hypochlorite (from household bleach, Sara Lee Ltd., New Zealand) was standardized by measuring A_{292} at pH 12 (ϵ_{292} 350 M^{-1} cm^{-1}) then diluted in PBS (137 mM NaCl in 10 mM phosphate buffer, pH 7.4). HOBr was prepared by adding HOCl to a 1.6-fold molar excess of NaBr in PBS. Its concentration was determined by absorbance at pH 12 (ϵ_{329} 332 M^{-1} cm^{-1}). HOSCN was prepared from lactoperoxidase, sodium thiocyanate, and H_2O_2 as described (37). HOI was prepared by mixing equal volumes of 10 mM HOCl and 15 mM potassium iodide, and used within 2 min of mixing. The initial concentration of HOI was based on the assumption of 100% conversion of HOCl to HOI. Taurine chloramine and taurine bromamine were prepared by adding HOCl or HOBr with mixing to a 10-fold molar excess of taurine, and NH_2Cl by adding HOCl to a 10-fold excess of ammonium acetate. Concentrations were determined assuming 100% conversion of HOCl or HOBr. $NHCl_2$ was prepared by adding a 2-fold excess of HOCl to ammonium acetate in 20 mM phosphate, pH 5.5, at 4 °C. Its concentration was determined from the absorbance of the solution and ϵ_{294} 270 M^{-1} cm^{-1}. These oxidants were used immediately after preparation.

Neutrophils and stimulants

Human neutrophils were isolated from heparinized peripheral blood of healthy donors and an individual with severe MPO deficiency (24), with informed consent approved by the Southern Health and Disability Ethics Committee, New Zealand. Neutrophils were prepared by dextran sedimentation followed by Ficoll-Paque centrifugation and hypotonic lysis of contaminating erythrocytes (38) and resuspended in Hanks' buffered salt solution (HBSS; PBS containing 1 mM $CaCl_2$, 0.5 mM $MgCl_2$, and 1 mg/ml of glucose).

S. aureus (strain 502a, ATCC 27217) from overnight cultures was washed with PBS and opsonized by incubating with human serum (20% in HBSS) at 37 °C for 20 min immediately before use. Zymosan A (from *Saccharomyces cerevisiae*, Sigma) was prepared in advance for opsonization by sonicating and boiling, then stored in frozen aliquots (39). Within 2 h of use it was incubated with human serum (50% in HBSS) at 37 °C for 30 min, washed by centrifugation, and resuspended in HBSS (5 mg/ml for 3×10^8/ml).

To covalently attach SOD, zymosan (14 mg/ml) and 1-ethyl-3-(3-dimethylaminopropyl)carbodiimide hydrochloride (18 mg/ml) (ThermoFisher) were suspended in MOPS buffer (0.025 M, pH 6) and treated with SOD (320 μg/ml) according to the manufacturer's instructions. The zymosan-SOD particles were collected by centrifugation, washed, and resuspended in PBS (20 mg/ml). Attachment of active SOD was confirmed by the ability of the particles to inhibit cytochrome *c* reduction with xanthine oxidase as the source of superoxide. The zymosan-linked SOD was inactivated by incubating at 37 °C for 1.5 h with 20 mM diethyldithiocarbamate (40). Intraphagosomal superoxide production was detected using dihydroethidium and measuring its fluorescent oxidation products (30) by flow cytometry (excitation 488/emission 575).

Reactions of R19-S with oxidants

Reactions were typically performed with R19-S (10 or 20 μM in PBS) and HOCl or one of the other oxidants (usually either equimolar or at half the R19-S concentration) added while vortexing. Samples were analyzed by LC-MS or fluorescence was followed over time with a Varioskan Flash platereader (Thermo Scientific, Finland) using 515 nm excitation and 550 nm emission.

Measurement of HOCl production by stimulated neutrophils

Typically, neutrophils were stimulated by incubating at 1×10^6/ml in HBSS at 37 °C with either opsonized zymosan (2×10^7/ml) or *S. aureus* (1×10^7/ml). R19-S (10 μM) and other reagents were added 10 min before stimulation. For fluorimetry, incubations were performed in 96-well plates with gentle shaking. Fluorescence measurements (excitation 515/emission 550 nm) were recorded over 60 min. To analyze extracellular and intracellular fractions, aliquots from reaction mixtures were spun at 300 × *g* for 5 min, and the fluorescence of supernatants and resuspended cell pellets were analyzed. For flow cytometry, incubations were performed in tubes with end-over-end rotation. Samples were removed at intervals for analysis using an FC500 MPL flow cytometer (Beckman Coulter) with gating on the neutrophil population, and red fluorescence intensity was measured by 488 nm laser excitation and a 575 nm emission detector.

Live-cell imaging

Single phagosome production of HOCl was measured by live-cell fluorescence microscopy. Neutrophils in HBSS at 37 °C were allowed to settle on a 35-mm glass bottomed dish before stimulation by zymosan or *S. aureus*. R19-S and other additives were added 10 min prior to stimulation. Time-lapse images of Cy3 and DIC channels were taken every 10 s over 30 min using an Olympus IX81 live-cell inverted microscope equipped with an XM10 monochrome fluorescence charge-coupled device camera and Cell R software (Olympus Soft Imaging Solutions, Münster, Germany) with ×20 magnification, exposure 100 ms (Cy3) and 10 ms (DIC). The Cell R software was used to mea-

sure the fluorescence development of single phagosomes with time.

Mass spectrometry

For LC-MS analysis, 50-μl samples were loaded onto a Jupiter C18 HPLC column (150 × 2 mm, 5 μm, 100 Å, Phenomenex) and separated using a Surveyor HPLC system (Thermo Scientific) by running a gradient from 95% solvent A (0.1% formic acid in water) to 95% solvent B (0.1% formic acid in acetonitrile) over 7 min at 200 μl/min and a column temperature of 40 °C. Solvent B was held at 95% for 10 min followed by column equilibration for 8 min with 95% solvent A. The HPLC was coupled to an electrospray ionization source of a Velos Pro ion trap mass spectrometer (Thermo Scientific). Voltage was 4 kV, the temperature of the heated capillary was 275 °C, and the vaporizer temperature was 400 °C. MS data were acquired in positive ion mode between 3.5 and 20 min of each chromatographic run. The ions for R19, R19-S, R19-S dimer, R19-SO, and R19S-Cl were detected at m/z 415, 431, 430, 447, and 465, respectively.

R19 and R19S-Cl were measured in lysates of 1×10^6 stimulated neutrophils by LC-MS/MS. Neutrophils were lysed by three 10-s bursts on ice with a Sonic Ruptor 400 micro-tip sonicator (Omni International), and proteins were precipitated by the addition of 4× volume of ice-cold ethanol followed by spinning at 12,000 × g for 10 min. Supernatants were dried by vacuum evaporation, resuspended in 100 μl of 0.1% formic acid in water, and 45 μl was analyzed by LC-MS/MS. Full collision-induced dissociation-MS/MS spectra from m/z 200 to 2000 were acquired for R19 (415 m/z) and R19S-Cl (465 m/z). The window for precursor selection was 1 Da on either side of the m/z; the normalized collision energy was 45 and activation time 30 ms. Scan data were post-acquisition filtered for the −28 fragment (loss of an ethylene group) for each of the precursors and the resulting peak was integrated.

Author contributions—A. M. A. and L. V. A. formal analysis; A. M. A. and N. D. investigation; A. M. A. writing-original draft; L. V. A. validation; L. V. A., N. D., A. J. K., and C. C. W. writing-review and editing; N. D. methodology; A. J. K. and C. C. W. conceptualization; A. J. K. and C. C. W. supervision.

Acknowledgments—We are grateful to Kenny Chitcholtan and Andreas Königstorfer for imaging assistance and Judy McKenzie for flow cytometry expertise.

References

1. Hurst, J. K. (2012) What really happens in the neutrophil phagosome? *Free Radic. Biol. Med.* **53,** 508–520 CrossRef Medline
2. Klebanoff, S. J. (2005) Myeloperoxidase: friend and foe. *J. Leukoc. Biol.* **77,** 598–625 CrossRef Medline
3. Rosen, H., Klebanoff, S. J., Wang, Y., Brot, N., Heinecke, J. W., and Fu, X. (2009) Methionine oxidation contributes to bacterial killing by the myeloperoxidase system of neutrophils. *Proc. Natl. Acad. Sci. U.S.A.* **106,** 18686–18691 CrossRef Medline
4. Klebanoff, S. J., Kettle, A. J., Rosen, H., Winterbourn, C. C., and Nauseef, W. M. (2013) Myeloperoxidase: a front-line defender against phagocytosed microorganisms. *J. Leukoc. Biol.* **93,** 185–198 CrossRef Medline
5. Winterbourn, C. C., Kettle, A. J., and Hampton, M. B. (2016) Reactive oxygen species and neutrophil function. *Annu. Rev. Biochem.* **85,** 765–792 CrossRef Medline
6. Winterbourn, C. C., Hampton, M. B., Livesey, J. H., and Kettle, A. J. (2006) Modeling the reactions of superoxide and myeloperoxidase in the neutrophil phagosome: implications for microbial killing. *J. Biol. Chem.* **281,** 39860–39869 CrossRef Medline
7. Rosen, H., Crowley, J. R., and Heinecke, J. W. (2002) Human neutrophils use the myeloperoxidase-hydrogen peroxide-chloride system to chlorinate but not nitrate bacterial proteins during phagocytosis. *J. Biol. Chem.* **277,** 30463–30468 CrossRef Medline
8. Chapman, A. L. P., Hampton, M. B., Senthilmohan, R., Winterbourn, C. C., and Kettle, A. J. (2002) Chlorination of bacterial and neutrophil proteins during phagocytosis and killing of *Staphylococcus aureus*. *J. Biol. Chem.* **277,** 9757–9762 CrossRef
9. Painter, R. G., Valentine, V. G., Lanson, N. A., Jr, Leidal, K., Zhang, Q., Lombard, G., Thompson, C., Viswanathan, A., Nauseef, W. M., Wang, G., and Wang, G. (2006) CFTR Expression in human neutrophils and the phagolysosomal chlorination defect in cystic fibrosis. *Biochemistry* **45,** 10260–10269 CrossRef Medline
10. Green, J. N., Kettle, A. J., and Winterbourn, C. C. (2014) Protein chlorination in neutrophil phagosomes and correlation with bacterial killing. *Free Radic. Biol. Med.* **77,** 49–56 CrossRef Medline
11. Segal, A. W. (2005) How neutrophils kill microbes. *Annu. Rev. Immunol.* **23,** 197–223 CrossRef Medline
12. Foote, J. R., Levine, A. P., Behe, P., Duchen, M. R., and Segal, A. W. (2017) Imaging the neutrophil phagosome and cytoplasm using a ratiometric pH indicator. *J. Vis. Exp.* CrossRef
13. Chen, X., Lee, K. A., Ha, E. M., Lee, K. M., Seo, Y. Y., Choi, H. K., Kim, H. N., Kim, M. J., Cho, C. S., Lee, S. Y., Lee, W. J., and Yoon, J. (2011) A specific and sensitive method for detection of hypochlorous acid for the imaging of microbe-induced HOCl production. *Chem. Commun.* **47,** 4373–4375 CrossRef
14. Koide, Y., Urano, Y., Hanaoka, K., Terai, T., and Nagano, T. (2011) Development of an Si-rhodamine-based far-red to near-infrared fluorescence probe selective for hypochlorous acid and its applications for biological imaging. *J. Am. Chem. Soc.* **133,** 5680–5682 CrossRef Medline
15. Zhang, Z., Zheng, Y., Hang, W., Yan, X., and Zhao, Y. (2011) Sensitive and selective off-on rhodamine hydrazide fluorescent chemosensor for hypochlorous acid detection and bioimaging. *Talanta* **85,** 779–786 CrossRef Medline
16. Yan, Y., Wang, S., Liu, Z., Wang, H., and Huang, D. (2010) CdSe-ZnS quantum dots for selective and sensitive detection and quantification of hypochlorite. *Anal. Chem.* **82,** 9775–9781 CrossRef Medline
17. Tlili, A., Dupré-Crochet, S., Erard, M., and Nüsse, O. (2011) Kinetic analysis of phagosomal production of reactive oxygen species. *Free Radic. Biol. Med.* **50,** 438–447 CrossRef Medline
18. Schwartz, J., Leidal, K. G., Femling, J. K., Weiss, J. P., and Nauseef, W. M. (2009) Neutrophil bleaching of GFP-expressing Staphylococci: probing the intraphagosomal fate of individual bacteria. *J. Immunol.* **183,** 2632–2641 CrossRef Medline
19. Chen, X., Lee, K. A., Ren, X., Ryu, J. C., Kim, G., Ryu, J. H., Lee, W. J., and Yoon, J. (2016) Synthesis of a highly HOCl-selective fluorescent probe and its use for imaging HOCl in cells and organisms. *Nat. Protoc.* **11,** 1219–1228 CrossRef Medline
20. Pattison, D. I., and Davies, M. J. (2001) Absolute rate constants for the reaction of hypochlorous acid with protein side chains and peptide bonds. *Chem. Res. Toxicol.* **14,** 1453–1464 CrossRef Medline
21. Thomas, E. L., Grisham, M. B., and Jefferson, M. M. (1986) Cytotoxicity of chloramines. *Methods Enzymol.* **132,** 585–593 CrossRef Medline
22. Coker, M. S., Hu, W. P., Senthilmohan, S. T., and Kettle, A. J. (2008) Pathways for the decay of organic dichloramines and liberation of antimicrobial chloramine gases. *Chem. Res. Toxicol.* **21,** 2334–2343 CrossRef Medline
23. Green, J. N., Chapman, A. L. P., Bishop, C. J., Winterbourn, C. C., and Kettle, A. J. (2017) Neutrophil granule proteins generate bactericidal ammonia chloramine on reaction with hydrogen peroxide. *Free Radic. Biol. Med.* **113,** 363–371 CrossRef Medline

24. Kettle, A. J., and Winterbourn, C. C. (1994) Superoxide-dependent hydroxylation by myeloperoxidase. *J. Biol. Chem.* **269,** 17146–17151 Medline
25. Tidén, A. K., Sjögren, T., Svensson, M., Bernlind, A., Senthilmohan, R., Auchère, F., Norman, H., Markgren, P. O, Gustavsson, S., Schmidt, S., Lundquist, S., Forbes, L. V., Magon, N. J., Paton, L. N., Jameson, G. N., Eriksson, H., and Kettle, A. J. (2011) 2-Thioxanthines are suicide inhibitors of myeloperoxidase that block oxidative stress during inflammation. *J. Biol. Chem.* **286,** 37578–37589 CrossRef Medline
26. Forbes, L. V., Sjögren, T., Auchère, F., Jenkins, D. W., Thong, B., Laughton, D., Hemsley, P., Pairaudeau, G., Turner, R., Eriksson, H., Unitt, J. F., and Kettle, A. J. (2013) Potent reversible inhibition of myeloperoxidase by aromatic hydroxamates. *J. Biol. Chem.* **288,** 36636–36647 CrossRef Medline
27. Forbes, L. V., and Kettle, A. J. (2018) A multi-substrate assay for finding physiologically effective inhibitors of myeloperoxidase. *Anal. Biochem.* **544,** 13–21 CrossRef Medline
28. Kettle, A. J., and Winterbourn, C. C. (1988) Superoxide modulates the activity of myeloperoxidase and optimizes the production of hypochlorous acid. *Biochem. J.* **252,** 529–536 CrossRef Medline
29. Kettle, A. J., Maroz, A., Woodroffe, G., Winterbourn, C. C., and Anderson, R. F. (2011) Spectral and kinetic evidence for reaction of superoxide with compound I of myeloperoxidase. *Free Radic. Biol. Med.* **51,** 2190–2194 CrossRef Medline
30. Zhao, H., Kalivendi, S., Zhang, H., Joseph, J., Nithipatikom, K., Vásquez-Vivar, J., and Kalyanaraman, B. (2003) Superoxide reacts with hydroethidine but forms a fluorescent product that is distinctly different from ethidium: potential implications in intracellular fluorescence detection of superoxide. *Free Radic. Biol. Med.* **34,** 1359–1368 CrossRef Medline
31. Jiang, Q., and Hurst, J. K. (1997) Relative chlorinating, nitrating, and oxidizing capabilities of neutrophils determined with phagocytosable probes. *J. Biol. Chem.* **272,** 32767–32772 CrossRef Medline
32. Jiang, Q., Griffin, D. A., Barofsky, D. F., and Hurst, J. K. (1997) Intraphagosomal chlorination dynamics and yields determined using unique fluorescent bacterial mimics. *Chem. Res. Toxicol.* **10,** 1080–1089 CrossRef Medline
33. Winterbourn, C. C., and Kettle, A. J. (2013) Redox reactions and microbial killing in the neutrophil phagosome. *Antioxid. Redox Signal.* **18,** 642–660 CrossRef Medline
34. Li, X. J., Tian, W., Stull, N. D., Grinstein, S., Atkinson, S., and Dinauer, M. C. (2009) A fluorescently tagged C-terminal fragment of $p47^{phox}$ detects NADPH oxidase dynamics during phagocytosis. *Mol. Biol. Cell* **20,** 1520–1532 CrossRef Medline
35. Soubhye, J., Chikh Alard, I., Aldib, I., Prévost, M., Gelbcke, M., De Carvalho, A., Furtmüller, P. G., Obinger, C., Flemmig, J., Tadrent, S., Meyer, F., Rousseau, A., Nève, J., Mathieu, V., Zouaoui Boudjeltia, K., Dufrasne, F., and Van Antwerpen, P. (2017) Discovery of novel potent reversible and irreversible myeloperoxidase inhibitors using virtual screening procedure. *J. Med. Chem.* **60,** 6563–6586 CrossRef Medline
36. Zheng, W., Warner, R., Ruggeri, R., Su, C., Cortes, C., Skoura, A., Ward, J., Ahn, K., Kalgutkar, A., Sun, D., Maurer, T. S., Bonin, P. D., Okerberg, C., Bobrowski, W., Kawabe, T., *et al.* (2015) PF-1355, a mechanism-based myeloperoxidase inhibitor, prevents immune complex vasculitis and anti-glomerular basement membrane glomerulonephritis. *J. Pharmacol. Exp. Ther.* **353,** 288–298 CrossRef Medline
37. Nagy, P., Jameson, G. N., and Winterbourn, C. C. (2009) Kinetics and mechanisms of the reaction of hypothiocyanous acid with 5-thio-2-nitrobenzoic acid and reduced glutathione. *Chem. Res. Toxicol.* **22,** 1833–1840 CrossRef Medline
38. Segal, A. W., Dorling, J., and Coade, S. (1980) Kinetics of fusion of the cytoplasmic granules with phagocytic vacuoles in human polymorphonuclear leukocytes: biochemical and morphological studies. *J. Cell Biol.* **85,** 42–59 CrossRef Medline
39. Allen, L. H. (2007) Immunofluorescence and confocal microscopy of neutrophils. In *Neutrophil Methods and Protocols* (Quinn, M. T., DeLeo, F. R., and Bokoch, G. M., eds) pp. 273–287, Humana Press, Totowa, NJ
40. Heikkila, R. E. (1985) Inactivation of superoxide dismutase by diethyldithiocarbamate. In *Handbook of Methods for Oxygen Radical Research* (Greenwald, R. A., ed) pp. 387–390, CRC Press, Boca Raton, FL